Insights about the interaction of methotrexate loaded hydrophilic gold nanoparticles: spectroscopic, morphological and structural characterizations

Sara Cerra,[a,]* Roberto Matassa,[b] Ana Maria Beltrán, [c] Giuseppe Familiari,[b] Chiara Battocchio,[d] Igor Pis,[e] Fabio Sciubba,[a] Francesca A. Scaramuzzo,[f] Alessandra Del Giudice,[a] and Ilaria Fratoddi[a,]*

[a] Department of Chemistry, Sapienza University of Rome, P.le A. Moro 5, 00185 Rome, Italy

[b] Department of Anatomical, Histological, Forensic and Orthopaedic Sciences, Section of Human Anatomy, Sapienza University of Rome, Via A. Borelli 50, 00161, Rome, Italy.

[c] Departamento de Ingeniería y Ciencia de los Materiales y del Transporte, Escuela Politécnica Superior, Universidad de Sevilla, Virgen de África 7, 41011 Seville, Spain.

[d] Department of Sciences and CISDiC, Roma Tre University, via della Vasca Navale 79, 00146 Rome, Italy

[e] IOM CNR, Laboratorio TASC, S.S. 14 Km 163.5 AREA Science Park Basovizza, Trieste, Italy
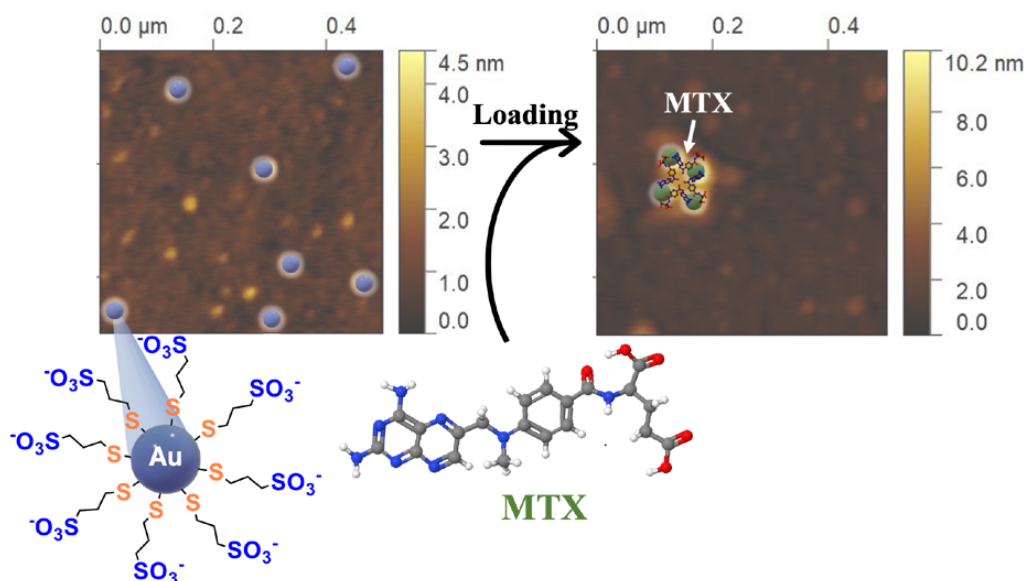
[f] Department of Basic and Applied Sciences for Engineering (SBAI), Sapienza University of Rome, Via Antonio Scarpa 14, 00161 Rome, Italy

Corresponding Author

*sara.cerra@uniroma1.it

*ilaria.fratoddi@uniroma1.it

Graphical abstract

The interaction between methotrexate drug and 3-mercapto-1-propanesulfonate functionalized gold nanoparticles was studied with the aim to highlight the overall structure of drug-loaded nanoparticles. The nature of interaction can be categorized into electrostatic binding between amine groups of MTX and negatively charged thiols on gold nanoparticles surface. This interaction results in a formation of large clusters with densely packed arrangement, as demonstrated by combined SAXS, HR-TEM and SR-XPS studies.

Highlights

- Functionalized AuNPs loaded with Methotrexate drug

- The physicochemical interaction between AuNPs and MTX was clarified

- AFM, SAXS and HR-TEM analyses highlighted the formation of densely packed clusters

- NMR and SR-XPS data indicated an interaction *via* electrostatic binding

Abstract

Gold nanoparticles (AuNPs) are promising carriers in the field of nanomedicine and represent a very intriguing approach in drug delivery applications, due to their small size and enhanced properties. This work aims to highlight the interaction between functionalized AuNPs and the immune-system suppressant drug Methotrexate (MTX) at molecular level. Small and monodisperse ($<2R_H>=5 \pm 1$ nm) gold nanoparticles were prepared by a simple chemical route using hydrophilic thiol 3-mercapto-1-propanesulfonate (3MPS) as a functionalizing/capping agent and act as a platform for post-synthesis conjugation of MTX *via* non-covalent interaction. The AuNPs-3MPS@MTX bioconjugate and the AuNPs alone were characterized to investigate their optical, chemical and morphological properties. Moreover, NMR, AFM, SAXS, HR-TEM and SR-XPS data confirmed the spherical shape of AuNPs and allowed to determine the mechanisms behind such drug-nanoparticle physicochemical interactions. These analyses define the overall structure of drug-loaded AuNPs-3MPS and drug location on the colloidal nanoparticles surface. Based on the experimental data, it is notable to assert that MTX was successfully loaded on the negatively charged nanoparticles surface *via* electrostatic interactions. The physicochemical behavior leads to the formation of large clusters with close packed arrangement of AuNPs-3MPS@MTX. This self-assembling property is of importance for delivery purpose affecting the drug-loaded nanoparticle size, functionality and morphology. Knowledge of how these systems behave will aid in increasing drug efficacy and in understanding the pharmacodynamics and pharmacokinetic properties, opening to new physicochemical insight for therapy and drug delivery systems.

Keywords: *hydrophilic nanoparticles; gold nanoparticles; methotrexate; drug delivery; structural characterization nanoparticles*

1. Introduction

Gold nanoparticles (AuNPs) are considered ideal materials for several applications, ranging from optoelectronics to biotechnology.[1-7] Recently, the interest towards gold nanoparticles in nanomedicine applications has greatly increased, especially with respect to drug delivery.[8-10] Aforementioned versatility lies in the possibility to fine-tune size, shape, surface potential and affinity with the medium, i.e. aqueous/organic solvents, as a function of chemical nature of stabilizing agent.[11] Many surface ligands are currently used, ranging from surfactants,[12] polymers,[13] block copolymers,[14] long-chain alcohols[15] to organometallics,[16] phosphanes,[17] amines,[18] thiols[19] and carboxylic acids.[20] Overall, thiol ligands confer to AuNPs stability towards aggregation thanks to the strong covalent gold-thiolate (RS-Au) bond[21,22] that confers both electrostatic and steric stabilization.[23,24] In general, hydrophobic thiolate protected AuNPs are useful to obtain colloids that are soluble in organic environment, while hydrophilic capping agents are used to produce water-soluble colloids. Although functionalized thiols were initially used to prevent nanoparticles aggregation, they were further used to control size, shape, metal-ligand interface as well as final properties of the obtained colloids.[25-27] The ease of surface functionalization allows the coupling with various biomolecules such as drugs,[28] nucleic acids,[29] fluorescent dyes,[30] polymers,[31] proteins[32] and peptides[33] onto nanoparticles. Moreover, high surface-to-volume ratio confers a high loading capacity.[34] AuNPs functionalized with hydrophilic thiols are well assessed in literature as biocompatible carriers for drugs with high molecular weight.[35,36] Methotrexate (MTX) is a folic acid antagonist which has been one of the most common drugs applied in the treatment of chronic inflammation of the epidermis.[37,38] MTX has shown immunosuppressive effects with regard to psoriasis and rheumatoid arthritis,[39,40] although side effects are present in case of oral administration.[41] Besides, transdermal delivery as topical

treatment represents viable alternative to oral delivery, but MTX owns a pH-dependent low solubility in water (<0.01 mg/mL at 20°C) which causes unsatisfactory percutaneous penetration.[42-44] To date, different delivery methods have been adopted in order to improve permeability of hydrophobic drugs through skin barrier respect to conventional therapeutic formulations.[45,46] AuNPs stabilized with sodium 3-mercapto-1-propanesulfonate (AuNPs-3MPS) have emerged as non-toxic materials for bioconjugation purposes.[9,10] Biological studies previously performed on these systems established that AuNPs-3MPS loaded with MTX are non-toxic carrier both *in vivo* and *in vitro*.[9,10] Tests on human keratinocytes (*in vitro* toxicity) and imiquimod-induced psoriasis-like mice model (*in vivo* toxicity) revealed not only the capacity of percutaneous adsorption and citocompatibility of small-sized AuNPs-3MPS but also AuNPs-3MPS@MTX ability to reduce keratinocytes hyperproliferation, epidermal thickness and inflammation of psoriatic plaques within 48 hours of treatment.[9,10] Herein, we present a detailed analysis on physicochemical characteristics of the conjugate AuNPs-3MPS@MTX. In addition, the intent of this study was to elucidate the interaction between AuNPs-3MPS and loaded MTX. In particular, UV-Vis, FT-IR, Dynamic Light Scattering (DLS), Nuclear Magnetic Resonance (NMR), Atomic Force Microscopy (AFM), Small-Angle X-ray Scattering (SAXS), High-Resolution Transmission Electron Microscopy (HR-TEM) and Synchrotron Radiation-induced X-ray Photoelectron Spectroscopy (SR-XPS) analyses were carried out on AuNPs-3MPS before and after interaction with MTX. The reported results represent a valuable background toward the full comprehension on the controlled nanoparticle-drug interaction, with biocompatibility relevance for studying chronic inflammation and drug response.

2. Experimental Section

2.1. Instruments

Ultraviolet–Visible (UV–Vis) absorption spectra were collected on a Varian Cary 100 spectrophotometer in the wavelength (λ) range 200–800 nm using quartz cells (optical path 1.00 cm, resolution 1 nm). Fourier Transform Infrared Spectroscopy (FTIR, Bruker Vertex 70) data were collected from 4000 to 400 cm^{-1} (16 scans at 4 cm^{-1} resolution) by Thallium Bromoiodide (KRS-5) pellet as Nujol mulls. Particle mean size, size distribution and zeta potential of the prepared AuNPs were measured in deionized water (18.3 MΩ·cm) at 25°C using a Dynamic Light Scattering device (DLS, Malvern Nano ZS90).

Further information on size and number concentration of AuNPs in suspension have been obtained by Small-Angle X-Ray Scattering measurements performed at SAXSLab Sapienza with a Xeuss 2.0 Q-Xoom system (Xenocs SA, Sassenage, France), equipped with a micro-focus Genix 3D X-ray Cu source ($\lambda = 0.1542$ nm), a two-dimensional Pilatus3 R 300K detector placed at variable distance from the sample (Dectris Ltd., Baden, Switzerland). Measurements were performed at room temperature (25±1°C) and in vacuo (pressure below 0.2 mbar), with three different sample-detector distances, in order to record the sample scattering within the scattering vector range of 0.045<q<10 nm^{-1} (q=4πsin(θ)/λ, where 2θ is the scattering angle). The samples were loaded in sealed glass capillaries. The two-dimensional scattering patterns were subtracted for the "dark" counts, and then masked, azimuthally averaged and normalized for transmitted beam intensity, exposure time and subtended solid angle per pixel, by using the FoxTrot software developed at SOLEIL. The one-dimensional Intensity *vs*. q profiles were then subtracted for the contributions of the water solvent and of the capillary and put in absolute scale units (cm^{-1}) by

dividing for the nominal capillary thickness 0.15 cm. Model calculations of scattering profiles were performed using the software SasView [www.sasview.org].

The morphological properties of the prepared colloids were studied by tapping-mode Atomic Force Microscopy (AFM, Veeco Instrument, Multimode™ model equipped with a Nanoscope IIIa controller, Bruker RTESP-300 probe). For the AFM analysis, AuNPs-3MPS and AuNPs-3MPS@MTX were deposited by drop casting onto a Si/SiO_2 substrate from its aqueous dispersion. High resolution TEM images were captured using FEI Talos F200S FEG microscope operating at 200 keV (CITIUS central services of the University of Seville, Spain). Compositional analysis was analyzed with a Super-X energy dispersive X-ray spectrometry system which includes two silicon drift detectors, couple to the microscope in the Scanning Transmission Electron Microscopy (STEM) mode, using spatial drift correction and a dwell time of 0.2 s.

The chemical interaction between the NPs surface and the capping agents was examined by Synchrotron Radiation-induced X-Ray Photoelectron Spectroscopy on drop casted samples onto a TiO_2 substrate from its aqueous dispersion and allowed to dry in clean conditions. SR-XPS measurements were carried out at the BACH (Beam line for Advanced DiCHroism) beamline at the ELETTRA synchrotron facility in Trieste (Italy).[47,48] XPS data were collected using a hemispherical electron energy analyzer (Scienta R3000, pass energy = 50 eV, angular mode) Photon energy of 360 eV was used for C1s, S2p, Au4f, spectral regions; for N1s and O1s spectral regions photon energy values of respectively 528 eV and 608 eV were selected, as to maximize signals intensities. The total energy resolution was 0.2 eV. The binding energy scale was calibrated using as reference the C1s aliphatic signal at 285 eV and the Au4f$_{7/2}$ signal of AuNPs arising by metallic gold atoms, always found at 83.96 eV. Curve-fitting analysis of the

C1s, S2p, N1s, O1s, Au4f spectra was performed using Gaussian curves as fitting functions. $S2p_{3/2}$, $S2p_{1/2}$ and $Au4f_{7/2}$, $Au4f_{5/2}$ doublets were fitted by using the same full width at half-maximum (FWHM) for each pair of components of the same core level, a spin–orbit splitting of 1.2 eV and 3.7 eV respectively, and branching ratios $S2p_{3/2}/S2p_{1/2} = 2/1$, $Au4f_{7/2}/Au4f_{5/2} = 4/3$. When several different species were individuated in a spectrum, the same FWHM value was used for all individual photoemission components.

NMR experiments were carried out on a Bruker Avance III spectrometer at 9.4T operating at a 400.13 MHz frequency for proton. The NPs were suspended in 0.6 ml of D_2O. Monodimensional ^1H experiments were acquired at 295K with 64k data points, a spectral width of 15 ppm, 16 scans and a repetition time of 6.55s in order to achieve full relaxation for all resonances. Bidimensional ^1H-^1H NOESY experiments were acquired with a mixing time of 150 ms at 298 K, a spectral width of 15 ppm in both dimensions employing a matrix of 8k x 256 data points, a repetition time of 2s and 64 scans.

2.2. Materials

Tetrachloroauric acid (III) trihydrate ($HAuCl_4 \cdot 3H_2O$, 99.0%); sodium 3-mercapto-1-propanesulfonate ($HS(CH_2)_3SO_3Na$, 3MPS, 90%); sodium borohydride ($NaBH_4$); methotrexate ($C_{20}H_{22}N_8O_5$, 4-Amino-10-methylfolic acid hydrate, MTX, ≥98%) and hydrochloric acid (HCl, ≥37%) were Sigma-Aldrich products. All chemicals were used without further purification. Ultra-pure water (18.3 MΩ·cm) was produced with a Zeener Power I Scholar-UV (Full Tech Instruments) deionization/purification apparatus.

2.3. Methods

2.3.1 Preparation of AuNPs-3MPS nanoparticles

In this study, AuNPs-3MPS with DLS mean particles size 5 ± 1 nm were prepared following the procedure already assessed in literature:[9] 0.1000 g of $HAuCl_4 \cdot 3H_2O$ ($2.5 \cdot 10^{-4}$ mol) were dissolved in 10 mL of ultra-pure water. Subsequently, 10 mL water solution of 3MPS 0.1810 g ($1.0 \cdot 10^{-4}$ mol) in Au/S 1/4 molar ratio was added. Gold reduction was completed by adding drop wise an aqueous solution of sodium borohydride (0.0960 g, $2.5 \cdot 10^{-3}$ mol) under vigorous stirring at $+4°C$. The reaction was carried out in inert atmosphere after degassing with Ar for 2 hours. AuNPs-3MPS nanoparticles were purified by repeated washing in centrifuge (13,400 rpm, 20min, 2x with deionized water and 5x with HCl 1M) in order to eliminate unbound thiols. For the ζ-potential distribution and FT-IR analysis see Figure S1, Supporting Information.

2.3.2 Preparation of AuNPs-3MPS@MTX *bioconjugate*

The chemical strategy used for non-covalent bioconjugation of MTX onto nanoparticles surface was previously reported.[9] Freshly prepared aqueous solutions of AuNPs-3MPS (10 mg/mL) and methotrexate drug (2 mg/mL) were mixed, adjusting pH to 5.5 with HCl 0.01 M. The interaction reaction was performed at 25 °C for 4 hours in the dark, under constant stirring. Then, the conjugate was washed one time with deionized water (6 mL) at 13400 rpm for 30 minutes to remove free MTX. For FT-IR spectra of the obtained bioconjugate see Figure S2, Supporting Information. The percentage loading of MTX was assessed from the supernatant after the bioconjugation reaction by interpolation with a UV-Vis calibration curve at 302 nm ($\varepsilon_{302} = 19330$ M^{-1} cm^{-1}) (see Figure S3, Supporting Information). Drug loading efficiency was calculated as 80 $\pm$ 5% in agreement with previous studies.[9,10]

3. Results and Discussion

3.1 UV-Vis and NMR measurements

The preparation of the bioconjugate AuNPs-3MPS@MTX followed a three-step procedure as depicted in Figure 1(a). In the first step, AuNPs-3MPS were prepared according to synthetic strategy outlined above. Accordingly, thiols 3MPS were covalently linked to AuNPs in the process of formation. In the second step, AuNPs-3MPS was reacted with MTX solution at room temperature in order to achieve a good loading percentage onto nanoparticles surface. In the final step, the reaction mixture was subjected to purification step in centrifuge to remove the unbound drug. The formation of the bioconjugate AuNPs-3MPS@MTX has been supported with the change in maximum absorption (λ_{LSPR}) position. Figure 1(b) exhibits the UV-Vis absorption spectra of AuNPs-3MPS and AuNPs-3MPS@MTX (Au/MTX 5/1 molar ratio). The strong band observed in the range 500-600 nm corresponds to the localized surface plasmon resonance (LSPR) phenomena and as known, this band is related to colloidal state of gold.[49] The LSPR position and shape are linked to factors such as shape, size, composition of gold colloids and dielectric constant of the environment. It is interesting to note that the plasmon resonance red shifts from λ_{LSPR}= 520 nm to λ_{LSPR}= 570 nm after conjugation with MTX, sign of an increase in particle diameter of the AuNPs-3MPS@MTX. Furthermore, the value of full width at half-maximum (FWHM) is potentially a sensitive criterion for the measurement of polydispersity. In general, broadening in the absorbance band is promoted by an increasing in the degree of dispersion of the sample. As it can be seen, the lower value of FWHM=90 ± 7 nm is observed in case of AuNPs-3MPS while FWHM value rises to 186 ± 3 nm in presence of MTX onto nanoparticles surface, indicating that bioconjugation reaction conditions lead to the largest size distributed nanoparticles. As demonstrated in literature, several small molecule drugs such as

methotrexate exhibit a tendency to aggregation, this leads to the formation of molecular clusters or discrete nanostructures variable in size and shape. This phenomenon can occur not only in buffer/aqueous solutions but also in cell culture media. This behavior could be enhanced by presence of hydrophilic amino-ring with ionizable amine group and anionic moiety on 3MPS-functionalizing thiols.[50,51] Despite this aggregation behavior, *in vitro* and *in vivo* biological studies demonstrated that dermis and epidermis layers of the skin do not retain the nanoparticles and AuNPs-3MPS@MTX are not toxic in vitro skin model.[9,10]

Further, in order to investigate the microenvironment of nanoparticles in a non-destructive way ^{1}H-NMR experiments were conducted. Assignments of the ^{1}H-NMR in Figure 1(c) revealed peaks at 2.78 ppm (CH_2), 2.95 ppm (CH_2) e 2.07 ppm (CH_2) corresponding to 3MPS-functionalized nanoparticles protons.[52] The MTX proton resonances were the following: singlet at 8.55 ppm (H-7), doublet at 7.61 ppm (H-2',6'), doublet at 6.78 ppm (H-3',5'), broad singlet at 4.77 ppm (H-9), doublet of doublets at 4.23 ppm (CH α), singlet at 3.10 (CH_3), multiplet at 2.24 (CH γ) and multiplets at 2.07 and 1.95 (CH β). The study of the interactions between AuNPs-3MPS and MTX was carried out by 2D NOESY experiment in D_2O solution reported in Figure 1(d). Of great interest is the presence of dipolar cross peaks among the aromatic protons of MTX with the same sign of the diagonal resonances. This is very important since the sign of a NOESY cross peak is opposite to the sign of the NOE which regulate the magnetization transfer, and in this instance, the peaks are positive and thus the NOE is negative. Negative NOE is typical of large molecules or aggregates, and as such it is a clear indication of the anchorage of the MTX on the surface of AuNPs-3MPS. Moreover, it is possible to observe the lack of dipolar cross peaks among 3MPS resonances comparing this NOESY with the one acquired on pure AuNPs-3MPS.[52] This evidence suggests that the addition of MTX can alter the spatial arrangement of

3MPS, giving the thiol a greater rotational freedom. This is possible only if the MTX is on the AuNPs-3MPS surface and not inserted between adjacent 3MPS molecules. The latter hypothesis is also to be excluded due to a lack of cross peaks between the protons of the molecules, suggesting that the interaction between them is mainly electrostatic in nature.
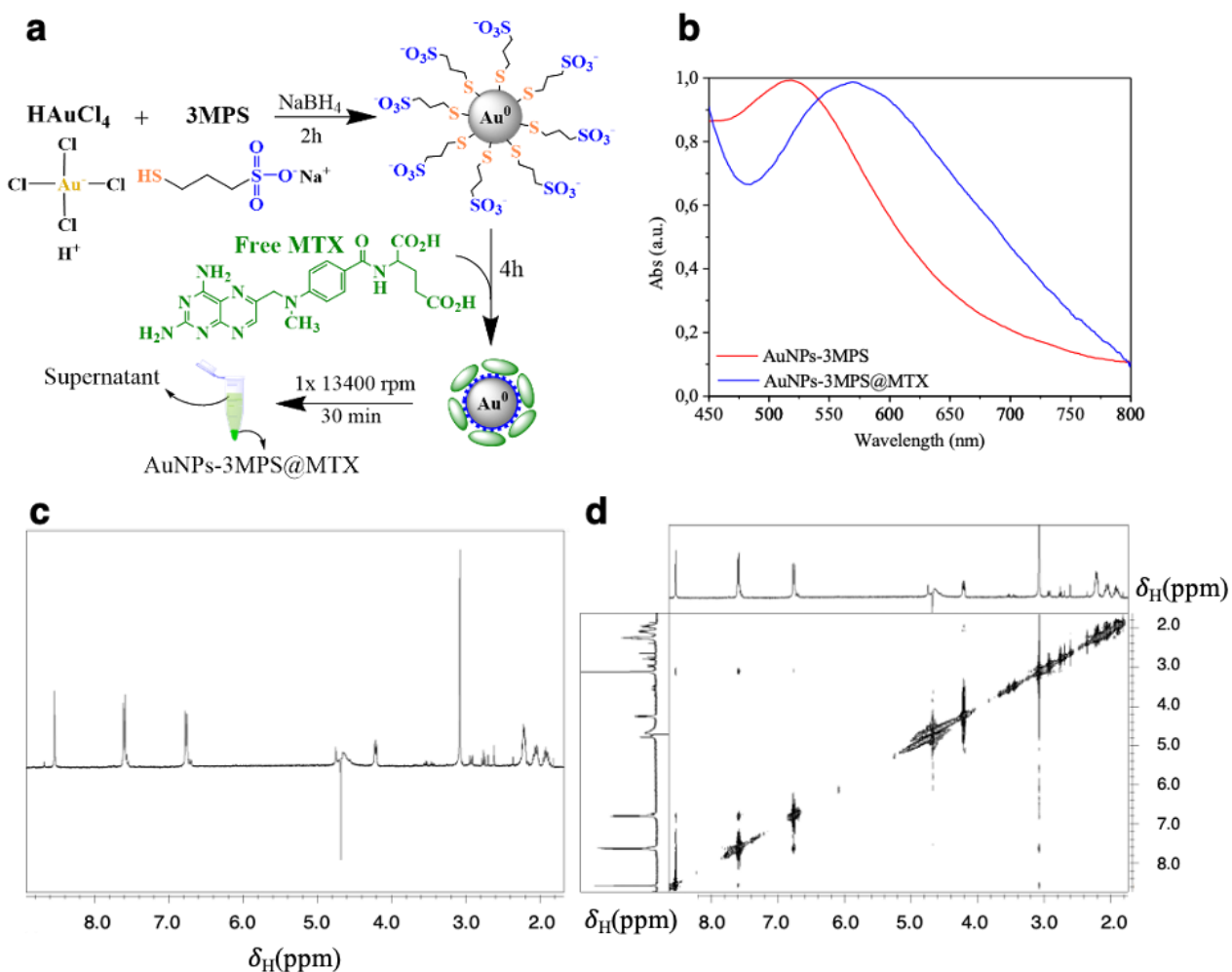
Figure 1. *(a) Reaction scheme of the synthesis of AuNPs-3MPS@MTX. (b) Normalized UV-Vis spectra of AuNPs-3MPS and AuNPs-3MPS@MTX in deionized water. (c) 1D ^{1}H-NMR spectra of the obtained bioconjugate. (d) 2D NOESY spectra of the obtained bioconjugate.*

3.2 DLS and SAXS analysis

The size and distribution of AuNPs-3MPS and AuNPs-3MPS@MTX were evaluated by DLS and SAXS. Figure 2 shows the hydrodynamic size distribution of colloidal samples diluted in deionized water. Red curve in Figure 2 shows the hydrodynamic size distribution of AuNPs-3MPS by Volume with $<2R_H>=5 \pm 1$ nm. Blue curve in Figure 2 shows hydrodynamic size distribution of AuNPs-3MPS@MTX with $<2R_H>=710 \pm 160$ nm. The results highlight a significant increment in the mean particle size of the colloid in the presence of MTX. This outcome suggests that AuNPs-3MPS tend to aggregate after the conjugation with drug molecules that may be induced from many factors such as surface coating and the physicochemical nature of the environment. As it is known in the literature, the red shift that occurs in UV-vis spectra and a slight increase of hydrodynamic radius can be related to a change in the local dielectric constant around gold nanoparticles as a result of MTX loading. This can have an impact on the interaction potential between the NPs which becomes less repulsive, leading to cluster formation.[53]
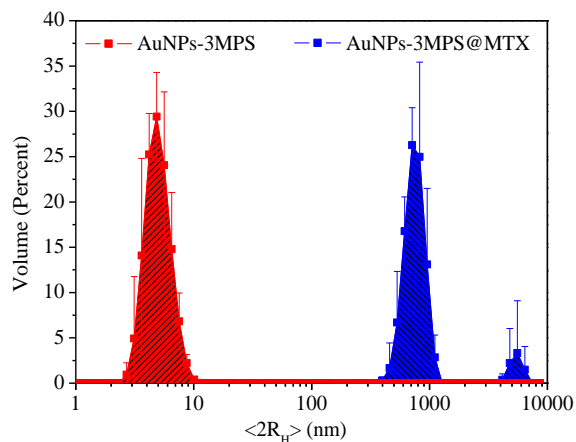
Figure 2. *Comparison of DLS measurements on AuNPs-3MPS before $<2R_H>=5 \pm 1$ nm (red curve) and after $<2R_H>=710 \pm 160$ nm (blue curve) the interaction with MTX.*

The SAXS analysis of the AuNPs-3MPS suspension provided a scattering profile in agreement with the expected size and shape of the nanoparticles: in particular the data could be fitted with the model intensity of a homogeneous sphere with radius 1.95 nm having the X-ray scattering length density of gold (1.25×10^{-2} nm^{-2}, considering a density of 19.3 g/cm^3), and a better agreement was achieved by introducing a polydispersity with a gaussian radius distribution centered at 1.60 nm and 25 % width (Figure 3(a)). A model considering a further spherical shell representing the 3MPS functionalization did not provide any improvement to the fitting, due to the negligible scattering cross-section of the ligand shell in SAXS compared to the very high electron density of Au. The ratio of the radius of gyration (R_g, from a Guinier fit of the data at low q, Figure 3(a) inset) and the hydrodynamic radius ($<R_H>$, from DLS) is around $R_g/R_H= 0.67$. This is lower than the theoretical value for hard spheres of 0.775, consistently with the negligible contribution to SAXS of the 3MPS shell, whereas this has an influence on the hydrodynamic radius measured by diffusion. Since the data were put on absolute units, from the volume fraction and the sphere radius obtained by the fitting with the monodisperse model, we could estimate a number density of roughly 2×10^{17} L^{-1}.
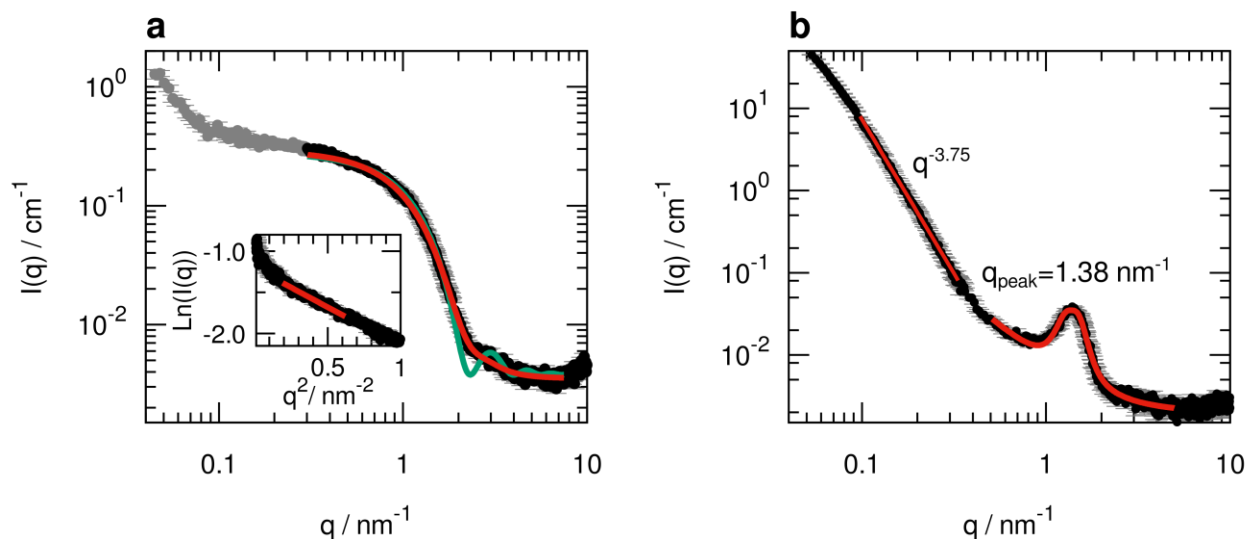
Figure 3. *(a) SAXS data of AuNPs-3MPS in water solution (dots with error bars); fit with model functions: monodisperse homogeneous sphere with radius 1.95 nm (green line), homogeneous sphere with radius 1.60 nm and 25% gaussian polydispersity (red line); in the inset the Guinier fit is shown giving a radius of gyration of 1.69 nm. (b) SAXS data of AuNPs-3MPS@MTX (dots with error bars); in the low q region a $q^{-3.75}$ slope was deduced; a broad peak centered at $q_{peak}=1.38$ nm^{-1} was found.*

The SAXS profile measured after the addition of MTX (Figure 3(b)) indicated nanoparticle aggregation into large clusters, with dimensions beyond the largest distance probed in the accessible q range, as already suggested by the DLS experiments. The SAXS scattered intensity strongly increased in the low q region, reaching an initial slope rather close to the q^{-4} expected for sharp interfaces according to the Porod law. This behavior can therefore be ascribed to the surface scattering (Porod) regime of the large aggregates. In addition, an evident correlation peak was detected at $q_{peak}=1.38$ nm^{-1}.[54] This corresponds to a close packed arrangement of the AuNPs-3MPS@MTX particles within the clusters.[55] The average particle–particle distance can be estimated from the peak position ($2\pi/q_{peak}$) to be 4.55 nm. This is slightly larger than the diameter estimated from the best fit radius (below 4 nm), which is consistent with the presence

of the ligand shell and possibly the added MTX. High resolution transmission electron microscopy provided further insights into the structure of these clusters, as discussed below.

3.3 Morphological characterization (AFM and HR-TEM)

AFM measurements show that pristine AuNPs-3MPS are characterized by an average height of around 4 nm. The particles show high grade of monodispersity and seem to be well detached from each other (Figures 4(a)-4(b)). A more quantitative information was achieved by performing a statistic on the height of a total number of 116 AuNPs-3MPS nanoparticles observed on randomly selected areas, whose resulting histogram is reported in Figure 4(c) (parameters of the Gauss fit are reported in Table S1, Supporting Information). On the other hand, after loading of MTX some aggregates appear. The organic monolayer thickness is too small to cause a meaningful change in the maximum height detectable with AFM, but the reported images suggest an interaction between the particles *via* the soft organic coating, absent in the previous case. Moreover, a thin amorphous layer is clearly visible on all the scanned surface (Figures 4(d)-4(e)).
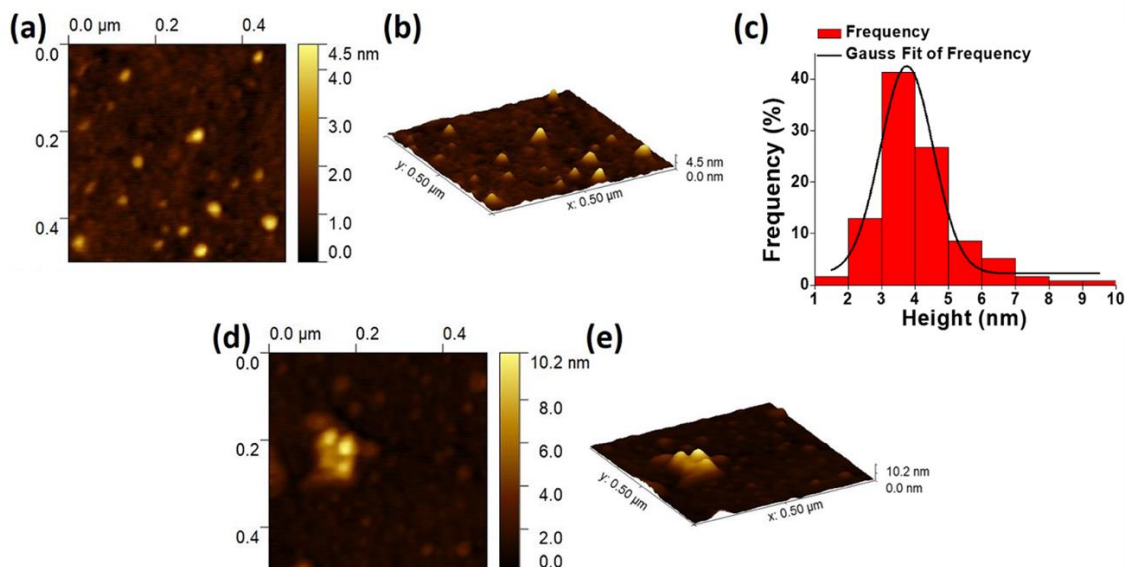
Figure 4. *(a) 2D and (b) 3D typical AFM images obtained for pristine AuNPs-3MPS deposited on Si/SiO$_2$. (c) Statistics of the distribution of AuNPs-3MPS z-dimensions obtained from collected AFM images over 116 particles. (d) 2D and (e) 3D typical AFM images obtained for AuNPs-3MPS@MTX deposited on Si/SiO$_2$.*

Detailed morpho-structural investigation of this hybrid material through electron microscopy technique have been performed at nanometric scale (Figure 5). The morphology and morphometric imaging of well separated AuNPs-3MPS forming an extensive bi-dimensional network are displayed in Figure 5(a). Appropriate imaging analyses have been exploited to perform accurate quantitative measurements of size–shape on a probed area of 121 nm by 121 nm.[56] The morphometric analysis has identified NPs of quasi-spherical shape with circularity of 0.86 ± 0.04. The broadening counts distribution has been fitted by a Gaussian distribution (GD) function to assess the measured diameter of the nanoparticles, providing an average value of 5.01 $\pm$ 0.04 nm with lowest polydispersity of about 1% (Inset Figure 5(a)). To identify the chemical composition of such dark NPs, energy dispersive X-ray spectroscopy technique (Figure S4, Supporting Information). The EDS nanoanalysis evidences the high purity of the aggregates,

17

showing intense energy peaks, belonging to gold specie (Cu, Fe, and Ni peaks were from instrumental background). The small sulfur peak, shoulder of Au emission line, may be noticed underling the presence of thiol groups covalently bound to the AuNPs-3MPS at the surface (see paragraph 3.4). High-resolution observations have been exploited for investigating the crystallinity behavior of the AuNPs-3MPS in presence of MTX. Figure 5(b) shows visible gold-sulfide nanocrystals and some nanometric region lacking lattice fringes depending on the defocus plane position. Several lattice planes with different d-*spacing* distances and orientation are shown, which indicates the random crystalline nature of the hybrid nanocrystals. By analyzing the HR-TEM images, the interplanar distances of the fringe were measured in agreement with the crystallographic lattice of gold sulfide (Au$_2$S) reported by Ishikawa *et al.*[57] This experimental result is also consistent with the low signal of the sulfur amount detected by EDS measurements (Figure S4, Supporting Information) The lattice fringes imaging revealed gold-sulfide nanocrystals with two different d-*spacing* of 0.290 nm and 0.247 nm, corresponding to the (111) and (002) planes (see Insets and arrows). The physicochemical interaction of the Methotrexate (MTX) with well-separated AuNPs-3MPS nanoparticles clearly shows a tendency to form a densely aggregate of overlapping NPs (Figure 5(c)). To get further details on the structure features, the Fast Fourier Transform (FFT) analysis has been performed on the HRTEM image in order to ascertain the presence of different crystalline phases (Inset).[58] By analogy to the nanodiffraction, the measured d-*spacing* of the diffraction rings were identified, confirming the presence of the Au$_2$S crystalline phase.[55] The strong signal of the diffraction rings indicated by orange arcs belongs to the cubic space group Pn3m in which the measured and calculated highest intensity signal belongs to the (111) diffraction plane with an interplanar spacing of d$_{111}$ = 0.290 nm. From the HR-TEM images, the image analysis through the sequence of FTT and Inverse

Fast Fourier Transform (IFTTs) elaboration were possible to discriminate wide lattice fringes of 0.492 nm probably due to the overlapping lattice nanocrystals (Moiré fringes), as a concrete evidence of clustering effect. Furthermore, it was possible to establish the mainly orientation of the plane lattice corresponding to the interplanar spacing of $d_{002} = 0.290$ nm. Therefore, the lattice fringe analyses also provide direct insight into the physicochemical processes leading to growth nanometric crystalline structures in a densely packed compacted aggregation due to the MTX presence.
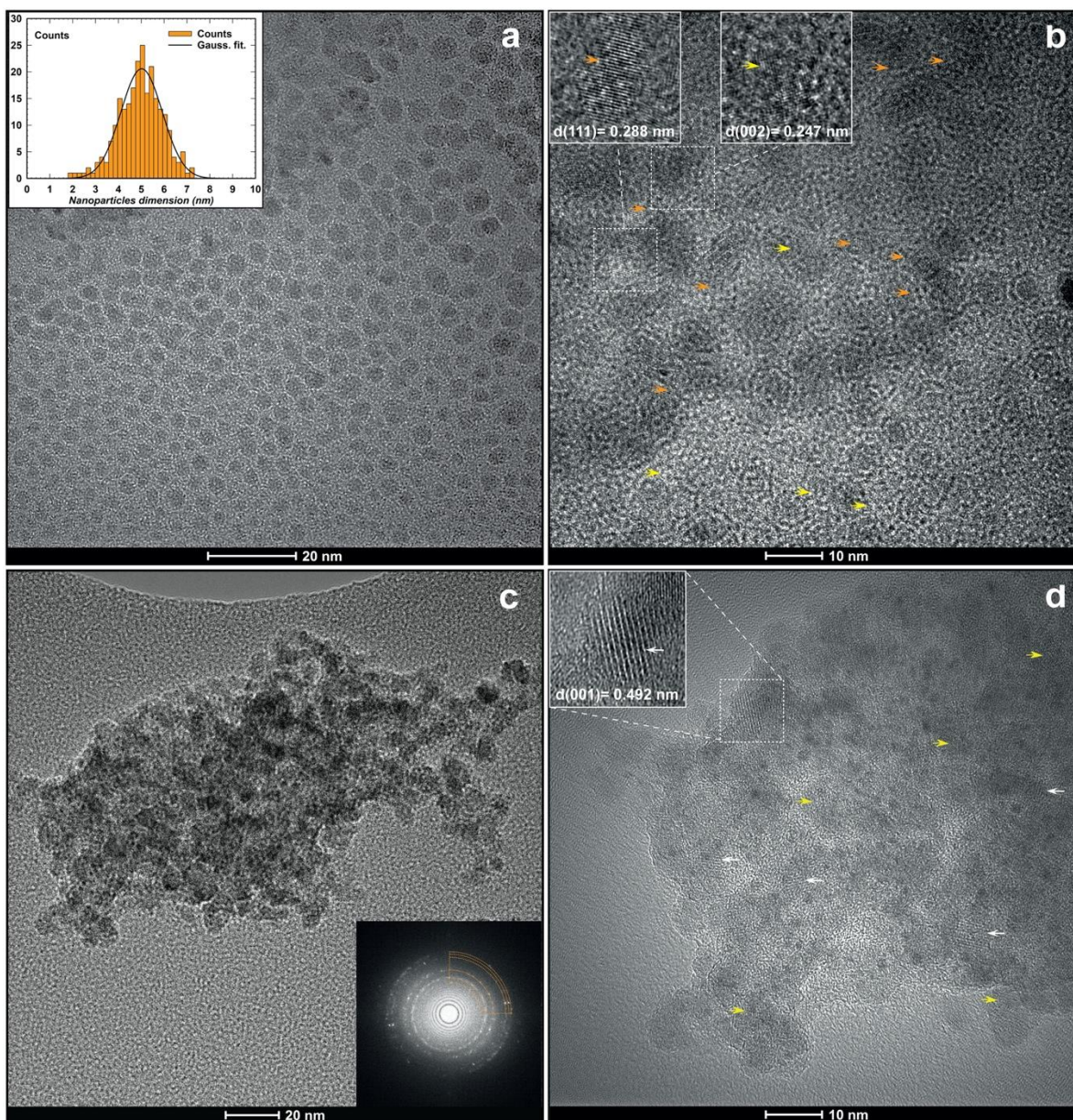
Figure 5. *Morpho-structural study of gold structured nanoparticles. (a) Bright field image of the inorganic–organic 2D-network of AuNPs-3MPS. Inset: plot showing the counts distribution of the nanoparticle size histogram. (b) HR-TEM image of gold-sulfide nanocrystals in AuNPs-3MPS, showing lattice fringe images of d-spacing 0.288 nm (orange arrows) and 0.247 nm (yellow arrows). (c) BF-TEM image of the densely packed 2D-network of AuNPs-3MPS interacted with MTX. Inset: FFT taken from Figure 5(c) showing distinct diffraction rings corresponding to the crystalline phases of Au$_2$S (orange dot line arcs). (d) HR-TEM image*

showing overlapping lattice fringes of Au₂S nanocrystallites of AuNPs-3MPS@MTX. Inset: typical Moiré fringe of 0.492 nm interplanar spacing.

3.4 SR-XPS

SR-XPS measurements were carried out with the aim to investigate the surface and interface chemical composition of AuNPs-3MPS@MTX, in comparison with the pristine AuNPs-3MPS. To evaluate the stability of the gold nanoparticles upon interaction with MTX, x-ray photoelectron spectra were collected at C1s, O1s, S2p, Au4f and N1s core levels and compared. Complete SR-XPS data analysis results (Binding Energy – BE, Full Width Half Maximum – FWHM, Atomic percentages and proposed assignments for all measured signals components) are reported in Table S1 in the Supporting Information.

S2p and Au4f core level spectra are the most indicative for the investigation of stabilizing molecule/metal interaction and were analyzed for both samples. As already reported for analogous AuNPs stabilized by 3MPS,[19] gold spectra show a main peak corresponding to metallic Au(0) of NPs bulk, and a small component at higher BE values (about 84.7 eV BE, 10% of whole Au4f signal intensity) attributed to gold atoms at the NP surface chemically interacting with the thiol moieties. On the other hand, S2p spectra have four spin-orbit pairs, attributed to: RS-Au (thiols covalently bound to gold atoms at the NP surface) ($S2p_{3/2}$ BE = 161.40 eV), physisorbed RS-H thiol groups ($S2p_{3/2}$ BE = 163.02 eV), and sulfonate functional groups ($S2p_{3/2}$ BE = 166.86, 168.46 for respectively $-SO_3^-$ and $-SO_3Na$). S2p and Au4f spectra are analogous for the two samples, confirming the stability of the 3MPS capping agent after the interaction with MTX. C1s, O1s and N1s signals gave interesting information about MTX loading and interaction with the stabilized gold nanoparticles. C1s spectra appear composite, and the spectral

components individuated by applying a peak fitting procedure are in agreement with the proposed molecular structure of both AuNPs-3MPS and AuNPs-3MPS@MTX, as reported in the "assignments" column of Table S1. More in detail, in AuNPs-3MPS@MTX sample a new C1s component appears, attributed to C-N groups, as expected. However, this feature is of very low intensity (3.1% of the whole C1s signal). O1s spectra of AuNPs-3MPS@MTX and AuNPs-3MPS are compared in Figure 6(a) and (b); as expected by the MTX chemical structure, a peak related to -OH groups appears in the MTX-containing sample spectrum (red component in Figure 6(a)).
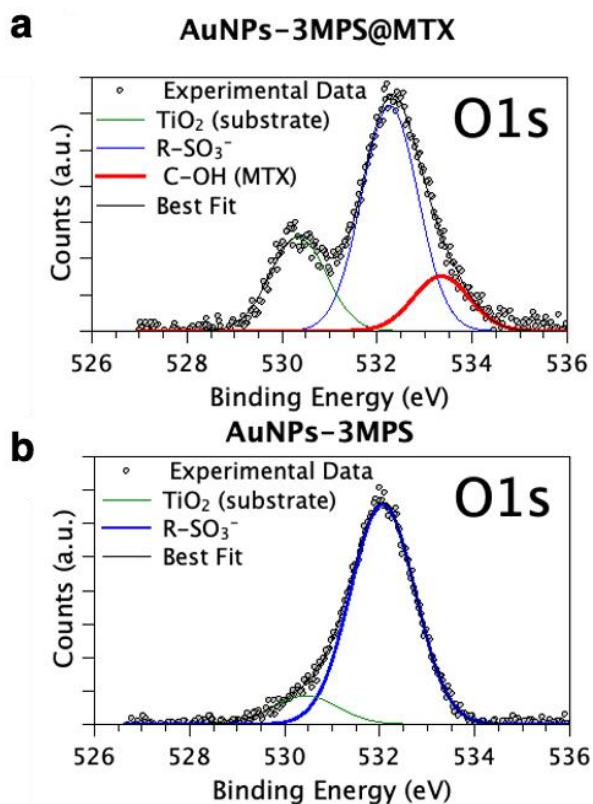
Figure 6. *O1s XPS spectra of (a) AuNPs-3MPS@MTX, (b) AuNPs-3MPS. The red component in spectrum (a) evidences the successful loading of AuNPs-3MPS with MTX.*

The most indicative signal for the investigation of the MTX/AuNPs-3MPS interaction is N1s spectrum. As reported in Figure 7, N1s spectrum of AuNPs-3MPS@MTX is composite and two main features can be individuated, in about 2:1 intensity ratio. Literature reports suggest that the peak at lower BE (398.60 eV) is associated with N atoms in the rings, as well as amide-like N atom and tertiary amines (since the typical BE values reported for these three different functional groups are not distinguishable with the here-used experimental resolution) (NIST X-ray Photoelectron Spectroscopy Database, Version 4.1 (National Institute of Standards and Technology, Gaithersburg, 2012; http://srdata.nist.gov/xps/)); the lower intensity signal at 401.6 eV BE is usually attributed to protonated amines ($R-NH_3^+$).[59] The observed intensity ratio between the two signals is in excellent agreement with the MTX molecular structure, hypothesizing that both $-NH_2$ groups are protonated.
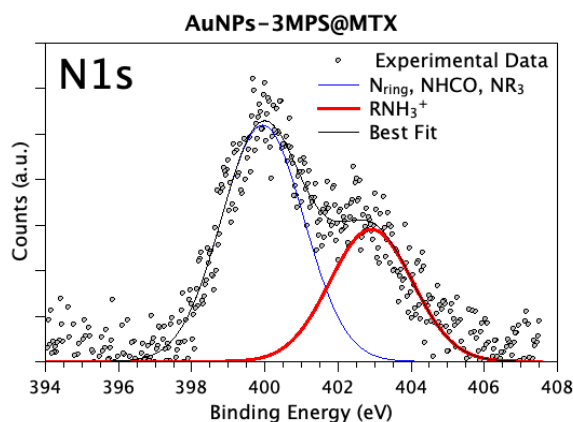
Figure 7. *N1s XPS spectrum of AuNPs-3MPS@MTX. The red component is related to protonated amine groups, that could interact with negatively charged sulfonate moieties of AuNPs-3MPS.*

SR-XPS data confirm the close packed arrangement of the AuNPs-3MPS@MTX particles within the clusters suggested by SAXS results; moreover, N1s core level spectral analysis allows to individuate the functional groups responsible for the MTX interaction with gold nanoparticles stabilized by the negatively charged 3MPS molecules.

4. Conclusions

In this work we shed light on the complex interactions between gold nanoparticles functionalized with 3MPS hydrophilic thiol and antifolate drug methotrexate, on the basis of previous studies that demonstrated its non-cytotoxicity and bioavailability in dermatological applications. To observe the behavior of MTX and AuNPs-3MPS, a fixed amount of AuNPs/MTX 5:1 molar ratio could interact in aqueous environment. Spectroscopic data together with surface analysis results confirmed the effective loading of the drug onto nanoparticles surface ($80 \pm 5\%$). The nature of AuNPs-3MPS and MTX interaction can be categorized into electrostatic binding between protonated aromatic -NH_2 groups in the ring structure of MTX and negatively charged -SO_3^- moieties of thiols capping agents, as confirmed by NMR and SR-XPS studies. Furthermore, isolated nanoparticles with $<2R_H>=5 \pm 1$ nm showed a tendency to aggregation up to $<2R_H>=710 \pm 160$ nm after addition of MTX as demonstrated by DLS, AFM and HR-TEM measurements. At the same time, electron microscopy and SAXS data revealed that the presence of methotrexate interacting electrostatically leads to a formation of large clusters with densely packed arrangement of AuNPs-3MPS@MTX. These results may contribute to the knowledge of physicochemical aspects behind drug-nanoparticles interactions which is a crucial aspect in optimization of drug carriers based on NPs properties.

ASSOCIATED CONTENT

Supporting Information. ζ-potential distribution and FT-IR characterization of AuNPs-3MPS (Figure S1). FT-IR spectra of AuNPs-3MPS@MTX (Figure S2). Calibration curve of MTX (Figure S3). EDS nanoanalysis of AuNPs-3MPS (Figure S4). Parameters of the histogram Gauss fit (Table S1). SR-XPS data of both AuNPs-3MPS and AuNPs-3MPS@MTX (Table S2).

Author Contributions

The manuscript was written through contributions of all authors. All authors have given approval to the final version of the manuscript.

Notes

The authors declare no competing financial interest.

References

1. Gad, G.M.A.; Hegazy, M.A. Optoelectronic Properties of Gold Nanoparticles Synthesized by Using Wet Chemical Method. *Mater Res. Express* **2019**, *6*, 085024.

2. Darienzo, R.E.; Chen, O.; Sullivan, M.; Mironava, T.; Tannenbaum, R. Au Nanoparticles for SERS: Temperature-Controlled Nanoparticle Morphologies and Their Raman Enhancing Properties. *Mater. Chem. Phys.* **2020**, *240*, 122143.

3. Xiao, T.; Huang, J.; Wang, D.; Meng, T. Au and Au-Based Nanomaterials: Synthesis and Recent Progress in Electrochemical Sensor Applications. *Talanta* **2020**, *206*, 120210.

4. Wu, Y.; Ali, M.R.; Chen, K.; Fang, N.; El-Sayed, M.A. Gold Nanoparticles in Biological Optical Imaging. *Nano Today* **2019**, *24*, 120-140.

5. Parise, C.; Ballarin, B.; Barreca, D.; Cassani, M.C.; Dambruoso, P.; Nanni, D.; Ragazzini, I.; Boanini, E. Gold Nanoparticles Supported on Functionalized Silica as Catalysts for Alkyne Hydroamination: A Chemico-Physical Insight. *Appl. Surf. Sci.* **2019**, *492*, 45-54.

6. Zhao, J.; Hu, X.; Huang, X.; Jin, X.; Koh, K.; Chen, H. A facile Gold Nanoparticles Embedded Hydrogel for Non-Enzymatic Sensing of Glucose. *Colloids Surf. B Biointerfaces* **2019**, *183*, 110404.

7. Fratoddi, I.; Rapa, M.; Testa, G.; Venditti, I.; Scaramuzzo, F.A.; Vinci, G. Response surface methodology for the optimization of phenolic compounds extraction from extra virgin olive oil with functionalized gold nanoparticles. Microchem. J. **2018**, *138*, 430-437.

8. Kong, F.-Y.; Zhang, J.-W.; Li, R.-F.; Wang, Z.-X.; Wang, W.-J.; Wang, W. Unique Roles of Gold Nanoparticles in Drug Delivery, Targeting and Imaging Applications. *Molecules* **2017**, *22*, 1445.

9. Bessar H.; Venditti I.; Benassi L.; Vaschieri C.; Azzoni P.; Pellacani G.; Magnoni C.; Botti E.; Casagrande V.; Federici M.; Costanzo A.; Fontana L.; Testa G.; Mostafa F.F.; Ibrahim S.A.; Russo M.V.; Fratoddi I. Functionalized Gold Nanoparticles for Topical Delivery of Methotrexate for The Possible Treatment of Psoriasis. *Colloids Surf. B Biointerfaces* **2016**, *141*, 141-147.

10. Fratoddi I.; Benassi L.; Botti E.; Vaschieri C.; Venditti I.; Bessar H.; Samir M.A.; Azzoni P.; Magnoni C.; Costanzo A.; Casagrande V.; Federici M.; Bianchi L.; Pellacani G. Effects of Topical Methotrexate Loaded Gold Nanoparticle in Cutaneous Inflammatory Mouse Model. *Nanomedicine* **2019**, *17*, 276-286.

11. Alex, S.; Tiwari, A.; Functionalized Gold Nanoparticles: Synthesis, Properties and Applications-A Review. *J. Nanosci. Nanotechnol.* **2015**, *15*, 1869-1894.

12. Lysyakova, L.; Lomadze, N.; Neher, D.; Maximova, K.; Kabashin, A.V.; Santer, S. Light-Tunable Plasmonic Nanoarchitectures Using Gold Nanoparticle−Azobenzene-Containing Cationic Surfactant Complexes. *J. Phys. Chem. C* **2015**, *119*, 3762−3770.

13. Liu, B.; Liu, J. Methods for Preparing DNA-Functionalized Gold Nanoparticles, a Key Reagent of Bioanalytical Chemistry. *Anal. Methods* **2017**, *9*, 2633-2643.

14. Seo, E.; Lee, S.H.; Lee, S.; Choi, S.H.; Hawker, C.J.; Kim, B.S. Highly Stable Au Nanoparticles with Double Hydrophilic Block Copolymer Templates: Correlation Between Structure and Stability. *Polym. Chem.* **2017**, *8*, 4528-4537.

15. Schmutzler, T.; Schindler, T.; Zech, T.; Lages, S.; Thoma, M.; Appavou, M.-S.; Peukert, W.; Spiecker, E.; Unruh, T. N-Hexanol Enhances the Cetyltrimethylammonium Bromide Stabilization of Small Gold Nanoparticles and Promotes the Growth of Gold Nanorods. *ACS Appl. Nano Mater*. **2019**, *2*, 3206-3219.

16. Gonzàlez de Rivera, F.; Angurella, I.; Rossella, O.; Secoa, M.; Llorca, J. Organometallic Surface Functionalization of Gold Nanoparticles. *J. of Organomet. Chem.* **2012**, *715*, 13-18.

17. Shichibu, Y.; Negishi, Y.; Tsukuda, T.; Teranishi, T. Large-Scale Synthesis of Thiolated Au_{25} Clusters via Ligand Exchange Reactions of Phosphine-Stabilized Au_{11} Clusters. *J. Am. Chem. Soc.* **2005**, *127*, 13464−13465.

18. Peng, S.; Lee, Y.; Wang, C.; Yin, H.; Dai, S.; Sun, S. A Facile Synthesis of Monodisperse Au Nanoparticles and Their Catalysis of CO Oxidation. *Nano Res.* **2008**, *1*, 229−234.

19. Carlini, L.; Fasolato, C.; Postorino, P.; Fratoddi, I.; Venditti, I.; Testa, G.; Battocchio, C. Comparison Between Silver and Gold Nanoparticles Stabilized with Negatively Charged Hydrophilic Thiols: SR-XPS and SERS as Probes for Structural Differences and Similarities. *Colloids Surf. A Physicochem. Eng. Asp.* **2017**, *532*, 183-188.

20. Rawat, K.A.; Kailasa, S.K. 4-Amino Nicotinic Acid Mediated Synthesis of Gold Nanoparticles for Visual Detection of Arginine, Histidine, Methionine and Tryptophan. *Sens. Actuators B Chem.* **2016**, *222*, 780-789.

21. Ulman, A.; Formation and Structure of Self-Assembled Monolayers. *Chem. Rev.* **1996**, *96*, 1533-1554.

22. Pensa, E.; Cortes, E.; Corthey, G.; Carro, P.; Vericat, C.; Fonticelli, M. H.; Benitez, G.; Rubert, A.A.; Salvarezza, R.C. The Chemistry of the Sulfur-Gold Interface: In Search of a Unified Model. *Acc. Chem. Res.* **2012**, *45*, 1183-1192.

23. Lin, S.-Y.; Tsai, Y.-T.; Chen, C.-C.; Lin, C.-M.; Chen, C.-H. Two-Step Functionalization of Neutral and Positively Charged Thiols onto Citrate-Stabilized Au Nanoparticles. *J. Phys. Chem. B* **2004**, *108*, 2134-2139.

24. Gao, J.; Huang, X.; Liu, H.; Zan, F.; Ren, J. Colloidal Stability of Gold Nanoparticles Modified with Thiol Compounds: Bioconjugation and Application in Cancer Cell Imaging. *Langmuir* **2012**, *28*, 4464-4471.

25. Azubel, M.; Kornberg, R.D. Synthesis of Water-Soluble, Thiolate-Protected Gold Nanoparticles Uniform in Size. *Nano Lett.* **2016**, *16*, 3348-3351.

26. Haes, A.J.; Zou, S.; Schatz, G.C.; Van Duyne, R.P. Nanoscale Optical Biosensor: Short Range Distance Dependence of the Localized Surface Plasmon Resonance of Noble Metal Nanoparticles. *J. Phys. Chem. B* **2004**, *108*, 6961-6968.

27. Balogh, L.; Nigavekar, S. S.; Nair, B. M.; Lesniak, W.; Zhang, C.; Sung, L. Y.; Kariapper, M. S. T.; El-Jawahri, A.; Llanes, M.; Bolton, B.; Mamou, F.; Tan, W.; Hutson, A.; Minc, L.; Khan, M. K. Significant Effect of Size On the In Vivo Biodistribution of Gold Composite Nanodevices in Mouse Tumor Models. *Nanomedicine* **2007**, *3*, 281−296.

28. Li, W.; Cao, Z.; Liu, R.; Liu, L.; Li, H.; Li, X.; Chen, Y.; Lu, C.; Liu, Y. AuNPs as an Important Inorganic Nanoparticle Applied in Drug Carrier Systems. *Artif. Cells Nanomed. Biotechnol.* **2019**, *47*, 4222-4233.

29. Carnevale, K.J.F.; Strouse, G.F. Intracellular DNA Cargo Release from a Gold Nanoparticle Modulated by the Nature of the Surface Coupling Functionality. *Bioconjug. Chem.* **2018**, *29*, 3429-3440.

30. Yu, J.; Qu, H.; Dong, T.; Rong, M.; Yang, L.; Liu, H. A Reversible Light-Responsive Assembly System Based on Host-Guest Interaction for Controlled Release. *New J. Chem.* **2018**, *42*, 6532-6537.

31. Banihashem, S.; Nezhati, M.N.; Panahi, H.A. Synthesis of Chitosan-Grafted-Poly(N-vinylcaprolactam) Coated on the Thiolated Gold Nanoparticles Surface for Controlled Release of Cisplatin. *Carbohydr. Polym.* **2020**, *227*, 115333.

32. Jazayeri, M.H.; Amani, H.; Pourfatollah, A.A.; Pazoki-Toroudi, H.; Sedighimoghaddam, B. Various Methods of Gold Nanoparticles (GNPs) Conjugation to Antibodies. *Sensing and Bio-Sensing Research* **2016**, *9*, 17-22.

33. Van Der Meer, S.B.; Loza, K.; Wey, K.; Heggen, M.; Beuck, C.; Bayer, P.; Epple, M. Click Chemistry on the Surface of Ultrasmall Gold Nanoparticles (2 nm) for Covalent Ligand Attachment Followed by NMR Spectroscopy. *Langmuir* **2019**, *35*, 7191-7204.

34. Wei, W.; Wei, M.; Liu, S. Silica Nanoparticles as a Carrier for Signal Amplification. *Rev. Anal. Chem.* **2012**, *31*, 163–176.

35. Fernández-Ponce, C.; Muñoz-Miranda, J.P.; de los Santos, D.M.; Aguado, E.; García-Cozar, F.; Litrán, R. Influence of Size and Surface Capping on Photoluminescence and Cytotoxicity of Gold Nanoparticles. *J. Nanopart. Res.* **2018**, *20*, 305.

36. Kalepu, S.; Nekkanti, V. Insoluble Drug Delivery Strategies: Review of Recent Advances and Business Prospects. *Acta Pharm. Sin. B* **2015**, *5*, 442–453.

37. Bedoui, Y.; Guillot, X.; Sélambarom, J.; Guiraud, P.; Giry, C.; Ja ar-Bandjee, M.C.; Ralandison, S.; Gasque, P. Methotrexate an Old Drug with New Tricks. *Int. J. Mol. Sci.* **2019**, *20*, 5023.

38. Morgado-Carrasco, D.; Fusta-Novell, X.; Riera Monroig, J.; Mascaro Galy, J.M. The METOP Study: Further Evidence for The Use of Subcutaneous Methotrexate in Psoriasis. *Actas. Dermosifiliogr.* **2017**, 108, 865–866.

39. Genestier, L.; Paillot, R.; Fournel, S.; Ferraro, C.; Miossec, P.; Revillard, J. P. Immunosuppressive Properties of Methotrexate: Apoptosis and Clonal Deletion of Activated Peripheral T cells. *J. Clin. Invest.* **1998**, *102*, 322-328.

40. Yélamos, O.; Puig, L. Systemic Methotrexate for The Treatment of Psoriasis. *Expert Rev. Clin. Immunol.* **2015**, *11*, 553-563.

41. Drach, M.; Papageorgiou, K.; Maul, J.T.; Djamei, V.; Yawalkar, N.; Häusermann, P.; Anzengruber F.; Navarini A.A. Effectiveness of Methotrexate in Moderate to Severe Psoriasis Patients: Real-World Registry Data from the Swiss Dermatology Network for Targeted Therapies (SDNTT). *Arch. Dermatol. Res.* **2019**, *311*, 753-760.

42. Brandt, J.V.; Piazza, R.D.; dos Santos, C.C.; Vega-Chacón, J.; Amantéa, B.E.; Pinto, G.C.; Magnani, M.; Piva, H.L.; Tedesco, A.C.; Primo, F.L.; Jafelicci, M.J.; Marques, R.F.C. Synthesis and Colloidal Characterization of Folic Acid-Modified PEG-b-PCL Micelles for Methotrexate Delivery. *Colloids Surf. B Biointerfaces* **2019**, *177*, 228-234.

43. Ray, S.; Joy, M.; Sa, B.; Ghosh, S.; Chakraborty, J. pH Dependent Chemical Stability and Release of Methotrexate from a Novel Nanoceramic Carrier. *RSC Adv.* **2015**, *5*, 39482.

44. Zhao, Y.; Guo, Y.; Li, R.; Wang, T.; Han, M.; Zhu, C.; Wang, X. Methotrexate Nanoparticles Prepared with Codendrimer from Polyamidoamine (PAMAM) and Oligoethylene Glycols (OEG) Dendrons: Antitumor Efficacy in Vitro and in Vivo. *Sci. Rep.* **2016**, *6*, 28983.

45. Du, H.; Liu, P.; Zhu, J.; Lan, J.; Li, Y.; Zhang, L.; Zhu, J.; Tao, J. Hyaluronic Acid-Based Dissolving Microneedle Patch Loaded with Methotrexate for Improved Treatment of Psoriasis. *ACS Appl. Mater. Interfaces* **2019**, *11*, 43588-43598.

46. Zeb, A.; Arif, S.T.; Malik, M.; Shah, F.A.; Din, F.U.; Qureshi, O.S.; Lee, E.-S.; Lee, G.-Y.; Kim, J.-K. Potential of Nanoparticulate Carriers for Improved Drug Delivery via Skin. *Int. J. of Pharm. Investig.* **2018**, *49*, 485-517.

47. Zangrando, M.; Zacchigna, M.; Finazzi, M.; Cocco, D.; Rochow, R.; Parmigiani, F. Polarized High-Brilliance and High-Resolution Soft X-Ray Source at ELETTRA: The Performance of Beamline BACH. *Rev. Sci. Instrum.* **2004**, *75*, 31–36.

48. Zangrando, M.; Finazzi, M.; Paolucci, G.; Comelli, G.; Diviacco, B.; Walker, R.P.; Cocco, D.; Parmigiani, F. BACH, the Beamline for Advanced Dichroic and Scattering Experiments at ELETTRA. *Rev. Sci. Instrum.* **2001**, *72*, 1313

49. Eustis, S.; El-Sayed, M.A. Why Gold Nanoparticles are More Precious than Pretty Gold: Noble Metal Surface Plasmon Resonance and its Enhancement of the Radiative and Nonradiative Properties of Nanocrystals of Different Shapes. *Chem. Soc. Rev.* **2006**, *35*, 209-217.

50. Ma, W.; Cheetham, A.G.; Cui, H. Building Nanostructures with Drugs. *Nano Today* **2016**, *11*, 13-30.

51. Owen, S.C.; Doak, A.K.; Wassam, P.; Shoichet, M.S.; Shoichet, B.K. Colloidal Aggregation Affects the Efficacy of Anticancer Drugs in Cell Culture. ACS Chem. Biol. **2012**, 7, 1429-1435.

52. Venditti, I.; Fontana, L.; Fratoddi, I.; Battocchio, C.; Cametti, C. Sennato, S.; Mura, F.; Sciubba, F.; Delfini, M.; Russo, M.V. Direct Interaction of Hydrophilic Gold Nanoparticles with Dexamethasone Drug: Loading and Release Study. *J. Colloid. Interface Sci.* **2014**, *418*, 52-60.

53. Chen, Y.-H.; Tsai, C.-Y.; Huang, P.-Y.; Chang, M.-Y.; Cheng, P.-C.; Chou, C.-H.; Chen, D.-H.; Wang, C.-R.; Shiau, A.-L.; Wu, C.-L. Methotrexate Conjugated to Gold Nanoparticles Inhibits Tumor Growth in a Syngeneic Lung Tumor Model. *Mol. Pharm.* **2007**, *4*, 713-722.

54. Lagrow, A. P.; Ingham, B.; Toney, M. F.; Tilley, R. D. Effect of Surfactant Concentration and Aggregation on The Growth Kinetics of Nickel Nanoparticles. *J. Phys. Chem. C* **2013**, *117*, 16709–16718.

55. Ingham, B.; Lim, T.H.; Dotzler, C.J.; Henning, A.; Toney, M.F.; Tilley, R.D. How Nanoparticles Coalesce: An In Situ Study of Au Nanoparticle Aggregation and Grain Growth. *Chem. Mater.* **2011**, *23*, 3312–3317.

56. Zanotto, A.; Matassa, R.; Saladino, M.L.; Berrettoni, M.; Giorgetti, M.; Zamponi, S.; Caponetti, E. Cobalt Hexacyanoferrate-poly(methylmethacrylate) Composite: Synthesis and Characterization. *Mater. Chem. Phys.* **2010**, *120*, 118-122.

57. Ishikawa, K.; Isonaga, T.; Wakita, S.; Suzuki, Y. Structure and Electrical Properties of Au_2S. *Solid State Ion.* **1995**, *79*, 60–66.

58. Matassa, R.; Orlanducci, S.; Reina, G.; Cassani, M.C.; Passeri, D.; Terranova, M.L. Structural and Morphological Peculiarities of Hybrid Au/Nanodiamond Engineered Nanostructures. *Sci. Rep.* **2016**, *6*, 31163.

59. Secchi, V.; Franchi, S.; Ciccarelli, D.; Dettin, M.; Zamuner, A.; Serio, A.; Iucci, G.; Battocchio, C. Biofunctionalization of TiO_2 Surfaces with Self-Assembling Layers of Oligopeptides Covalently Grafted to Chitosan. *ACS Biomater. Sci. Eng.* **2019**, *5*, 2190-2199.

SUPPORTING INFORMATION
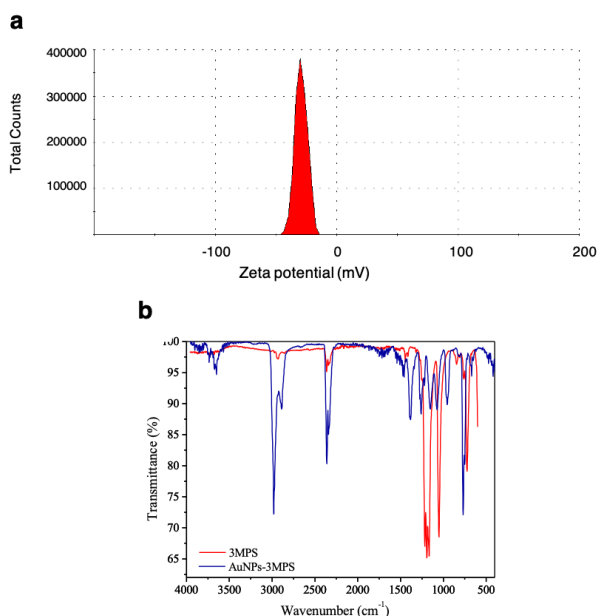
Figure S1. *(a) ζ-potential distribution = -29.3 ± 5 mV of AuNPs-3MPS in absence of MTX.*
(b) FT-IR analysis of AuNPs-3MPS (deposited from CHCl₃). The spectra revealed strong bands
associated to $v_{as}(-S=O)=1420\text{-}1300~cm^{-1}$, $v_s(-S=O)=1000\text{-}1200~cm^{-1}$ and $v(-S\text{-}O)=670~cm^{-1}$ of −
SO_3^- group. Weak band appears at 750 cm^{-1} due to $v(-C\text{-}S)$ of 3MPS.The sharp peaks at 2891
cm^{-1} and 2979 cm^{-1} are attributable to $v_{as}(-C\text{-}H)$ and $v_s(-C\text{-}H)$ of the aliphatic chain of 3MPS,
*respectively.*
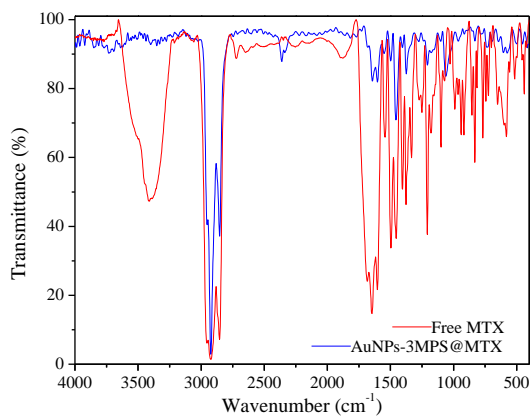
Figure S2. *Comparison of FT-IR spectra (nujol mull) of AuNPs-3MPS@MTX and free MTX.*
The spectrum of AuNPs-3MPS@MTX shows a characteristic band attributable to $v(-OH)=3390$

31

cm^{-1}, $v(-C=O)=1600\ cm^{-1}$ and $1643\ cm^{-1}$, the band is splited into a doublet due to the stretching of $-CO_2H$ and $-C(O)NH-$ functional groups of MTX. $\delta(N-H)$ of amidic group appear in the range $1550-1500\ cm^{-1}$, partially overlapping with the aromatic in-ring $v(-C=C-)$. Another remarkable bands are $v_{as}(S=O)=1374\ cm^{-1}$ and $v_s(S=O)=1060\ cm^{-1}$ due to the presence of 3MPS groups functionalizing AuNPs.
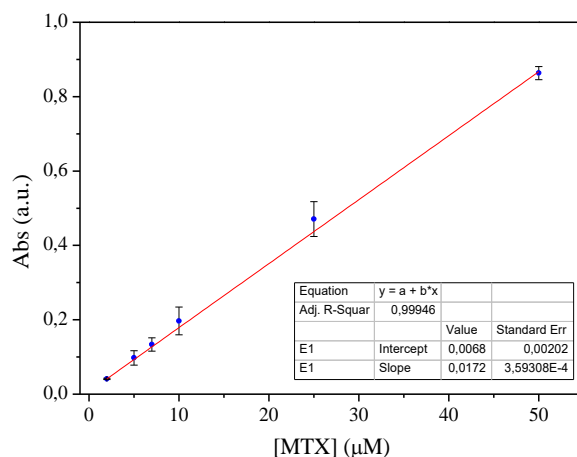
Figure S3. *Calibration curve of MTX.*
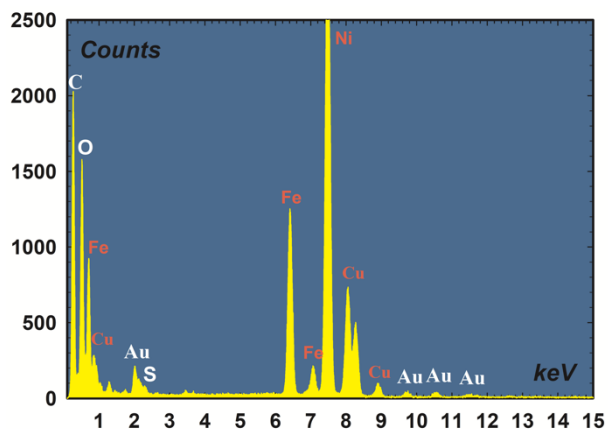
Figure S4. *EDS nanoanalysis of AuNPs-3MPS.*

Table S1. Parameters of the histogram Gauss fit.		
Equation: y=y0 + (A/(w*sqrt(PI/2)))*exp(-2*((x-xc)/w)^2)		
Adj. R-Square: 0.9750		
	Value	Standard Error
y0	2.27	1.02
xc	3.75	0.05
w	1.57	0.12
A	79.56	6.25
sigma	0.79	
FWHM	1.85	
Height	40.34	

Table S2. SR-XPS data collected on AuNPs-3MPS and AuNPs-3MPS@MTX.					
sample	signal	BE (eV)	FWHM (eV)	assignments	Atomic percent (%)
AuNPs-3MPS	C1s	285.00	1.21	C-C	90.1
		286.16	1.21	C-S, C-O-C	7.3
		287.44	1.21	C=O	1.5

		289.07	1.21	COOH	1.1
	O1s	530.76	1.86	TiO$_2$	
		532.39	1.86	-SO$_3^-$	
	S2p	161.40	1.48	RS-Au	6.7
		163.02	1.48	RS-H	42.5
		166.86	1.48	R-SO$_3^-$	15.6
		168.46	1.48	R-SO$_3$Na	35.2
	Au4f	83.96	0.63	Au(0)	90.7
		84.72	0.63	Au(δ^+)	9.3
AuNPs-3MPS@MTX	C1s	285.00	1.11	C-C	87.4
		286.01	1.11	C-S, C-O-C	7.3
		286.95	1.11	C-N	3.1
		288.00	1.11	C=O	1.1
		289.12	1.11	COOH	1.1
	N1s	398.60	2.65	N$_{ring}$, NHCO, NR$_3$	64.2
		401.57	2.65	RNH$_3^+$	35.8
	O1s	530.39	1.40	TiO$_2$	24.3
		532.33	1.40	-SO$_3^-$	59.4
		533.35	1.40	-OH	16.3
	S2p$_{3/2}$	161.40	1.43	RS-Au	12.5
		163.09	1.43	RS-H	48.1
		165.50	1.43	R-SO$_3^-$	6.8
		168.23	1.43	R-SO$_3$Na	32.6
	Au4f$_{7/2}$	83.96	1.31	Au(0)	90.6

		85.22	1.31	Au(δ^+)	9.4